DOE/BC/14850--1

RESERVOIR ENGINEERING RESEARCH INSTITUTE

Research Program on Fractured Petroleum Reservoirs

DE-FG22-96BC14850

July 31, 1996

Contract Date: March 25, 1996

DOE Program Manager: Dr. Robert E. Lemmon

Principal Investigator: Dr. Abbas Firoozabadi

DOE/BC/14850

2Q.96

April 1, 1996 - June 30, 1996

845 Page Mill Road
Palo Alto, CA 94304
(415) 424-8833

DISCLAIMER

DISCLAIMER

RESERVOIR ENGINEERING RESEARCH INSTITUTE

TASK II - NEW PHASE FORMATION AND FLOW IN POROUS MEDIA

A Phenomenological Network Modeling of
Critical Condensate Saturation

2Q.96

April 1 - June 30, 1996

Fang Fang

Abbas Firoozabadi

in collaboration with

Magsoud Abbaszadeh, Japan National Oil Corporation

Clay J. Radke, University of California, Berkeley

A Phenomenological Network Modeling of Critical Condensate Saturation

Abstract

We have developed a phenomenological model for critical condensate saturation. This model reveals that critical condensate saturation is a function of surface tension and contact angle hysteresis. On the other hand, residual oil saturation does not have such a dependency. Consequently, the selection of fluids in laboratory measurements for gas condensate systems should be made with care.

Introduction

Gas condensate reservoirs are becoming increasingly important; many new hydrocarbon reservoirs found in recent years are gas condensate reservoirs. These reservoirs, from a recovery and deliverability standpoint, may have significant differences from oil reservoirs. Prior to reaching the dew point pressure, the flow of gas in porous media is similar to that of undersaturated oil. When the pressure, either in the wellbore, or in the reservoir, drops below the dew point pressure, a new liquid condensate phase appears. The saturation of the new phase has to reach a threshold value in order to become mobile, provided the surface tension is higher than a critical value [1] (say $\sigma \geq 0.01$ dyne/cm). This threshold value is called critical condensate saturation, S_{cc}. When $\sigma < \sigma_c$, the critical contact angle, $\theta_c = 0°$ and therefore the liquid condensate will perfectly wet the rock. The phenomenon of critical point wetting [1] for a near critical condensate fluid in porous media is very complicated due to the chemical heterogeneousness of the rock surface and the presence of the interestial water [2]. For $\sigma < \sigma_c$, the new liquid phase spreads as a thin liquid film and film flow may occur. Consequently, S_{cc} may be very low, say less than 1 to 2 percent. For $\sigma > \sigma_c$, which is often the case, the new liquid phase is hypothesized to form liquid bridges between the walls of the pore network. For this case, the corresponding S_{cc} may be high.

The formation of a new gas phase, when the pressure of an undersaturated oil is lowered below the bubble point pressure, is followed by critical gas saturation, S_{cr}. There are fundamental differences between S_{cc} and S_{cr}. Critical gas saturation develops from the bubble nucleation in porous media [3] and its value is often of the order of 1 to 5 percent. Critical condensate saturation results from retrograde condensation in porous media, and the measured values are in the range of 10 to 50 percent [4-8]. Such high values may imply that critical condensate saturation could be similar to residual saturation in oil reservoirs. Residual oil saturation, S_{or}, is established by displacement. Since S_{cc} results from the in-situ liquid formation, and S_{or} is established by displacement, it is reasonable to believe that they are two different entities. S_{or} is not sensitive to the surface tension. It stays constant with increasing surface tension above a certain value. However, the dependency of S_{cc} on surface tension is unknown. It is also highly desirable to examine the relationship between surface tension, gravity and critical condensate saturation. Currently there is no theoretical model for critical condensate saturation. The main purpose of this work is to develop a phenomenological model to understand the effect of surface tension and gravity on S_{cc}.

We have embarked on a theoretical investigation for the understanding of: 1) the mechanisms of in-situ liquid formation and flow, and 2) the difference between two-phase flow from external displacement and from in-situ liquid formation (internal). The first objective is mainly to address S_{cc}, and the second objective is well deliverability of gas condensate reservoirs. In this paper, the results of the work on S_{cc} will be presented.

S_{or} in a single tube

It is well known that in a single tube, S_{or} and the P_c-S_w relationship depend on the shape of the tube. Refs. 9 to 12 provide the capillary pressure saturation relationships for the circular, triangular, rectangular and curved triangular cross-section tubes. **Fig. 1** displays various plots of the imbibition capillary pressure.

For a circular capillary tube of radius r, filled with a liquid and immersed in another fluid, if $P_c > 2\sigma\cos\theta / r$ is imposed, the tube will become empty; consequently, the concept of residual saturation does not apply to a capillary tube with a circular cross-section. The tube can be either empty or full.

Fig. 1a shows the imbibition capillary pressure-saturation for a triangular tube where $P_c / (\sigma / a)$ is the dimensionless capillary pressure, and a is the side length of the triangle. Note that residual nonwetting phase saturation, S_{or}, (shown by an open circle) is independent of the surface tension while capillary pressure, P_c, increases with surface tension.

The imbibition P_c-S_w results for a square tube are shown in **Fig. 1b**. Parameter x on the

y-axis denotes the side length of the square. Similar to a triangular tube, residual nonwetting phase saturation, S_{or}, is independent of the surface tension and changes with contact angle..

The imbibition P_c - S_w relationship for a curved triangular tube which incorporates pore angularity is different from the shapes of triangular and rectangular tubes. Princen reasons that pore angularity is an important element of capillary pressure in porous media.[11] The examination of the P_c - S_w plot shown in **Fig. 1c** (r is the radius of the side curve) reveals both positive and negative P_c for $\theta = 75°$, but similar to previous shapes, S_{or}, is independent of the surface tension.

S_{cc} in a single tube

In the following, we will establish that the liquid holdup (i.e., critical condensate saturation, S_{cc}) in various tube geometries from the in-situ liquid formation, has features which are different from S_{or}.

Circular cross-section tube. Consider a circular capillary tube of radius r shown in **Fig. 2.** Assuming in-situ liquid condensation of height h in the tube, the force balance on the liquid column gives:

$$P_R - P_A = \frac{2\sigma}{r}(\cos\theta_R - \cos\theta_A) - \Delta\rho g h \text{ .... (1)}$$

where subscripts R and A stand for receding and advancing interfaces (i.e., θ_R receding contact angle), and P_R and P_A represent the pressures on the gas sides. In case of contact angle hysteresis, $\theta_A > \theta_R$. (The dashed interfaces in **Fig. 2** have the same contact angle)

The liquid column will flow only when

$$h \geq \frac{2\sigma}{\Delta\rho g r}(\cos\theta_R - \cos\theta_A) - \frac{(P_R - P_A)}{\Delta\rho g} \quad \text{..............} \quad (2)$$

Assuming the gas pressure difference on both sides of the liquid column to be small, $P_R - P_A \cong 0$, then Eq. 2 implies that if $\theta_R = \theta_A$, no matter how small the liquid height and how large the surface tension are, the liquid will flow. It also reveals that critical condensate saturation in a bundle of capillary tubes, 1) increases with an increase in the surface tension, 2) increases with the decrease in the diameter, and 3) increases with an increase in the contact angle hysteresis (the difference between the advancing and the receding contact angle).

Triangular cross-section tube. The height of the liquid column from the in-situ condensation in a triangular-shaped tube is given by (see **Figs. 3b and 4**)

$$h = \frac{4\sqrt{3}\sigma}{\Delta\rho g a}(\cos\theta_R - \cos\theta_A) \quad \text{........................} \quad (3)$$

where gas pressure is assumed to be constant at both ends of the liquid column (see the derivation in the appendix). From the above equation, we note that the amount of liquid that a triangular-shaped tube can hold is also proportional to surface tension and is related to contact angle hysteresis which is similar to a circular tube.

Curved triangular cross-section tube. The height of the liquid holdup in a curved triangular tube is given by (see **Figs. 3c and 4**)

$$h=\frac{\sigma}{\Delta\rho gr}[\frac{(l_{1R}\cos\theta_R+l_{2R})}{A_R/r}-\frac{(l_{1A}\cos\theta_A+l_{2A})}{A_A/r}] \quad ... (4)$$

The parameters l_{1R}, l_{2R}, l_{1A}, l_{2A}, A_R and A_A are defined in the appendix together with the derivation of Eq. 4. In the above equation, similar to Eq. 3, the critical condensate saturation depends on the surface tension and the areal size of the tube. It is also related to the contact angle hysteresis.

A simple calculation may be useful to appreciate which of the tube geometries will hold more liquid. Let's assume $\sigma=2\ dynes/cm$, $\Delta\rho=0.3\ g/cm^3$, $\theta_R=0°$, $\theta_A=10°$ and the cross-sectional area of the tube $=1\ \mu m^2$. For a circular tube, $r=0.56\ \mu m$, and Eq. 2 provides $h=3.6\ cm$; for a triangular tube, $a=1.52\ \mu m$, from Eq. 3, $h=4.64\ cm$; for a curved triangular tube, from Eqs. A-12 and 4, $\alpha_A=30°$, $\alpha_R=28.65°$ and $h=7.5\ cm$. Therefore, the curved triangular tube can hold more liquid than circular or triangular tubes.

S_{cc} in a network

A variety of network configurations and shapes are used to represent porous media. In this work, we use a very simple network composed of vertical interconnected circular capillary tubes. A size distribution for the network can be assigned. To model the condensate formation and flow in a network, since there are no existing rules for in-situ liquid phase formation, we have to establish such rules for both a single tube and intersections of the network. Theoretical considerations will guide us towards this end.

Liquid forming in a single tube. Consider two capillary tubes with radii r_1 and r_2; assume $r_1 < r_2$. The vapor pressure of a pure component in tube r_1 will be less than in tube r_2. The decrease in vapor pressure for a curved interface is well known; the Kelvin equation provides the relationship between the vapor pressure and the interface curvature [13]. However, for hydrocarbon mixtures, the saturation pressure often increases as the interface curvature increases. In other words, the saturation pressure in tube r_1 will be more than the saturation pressure in tube r_2. The effect of curvature on the saturation pressure of hydrocarbon mixtures is discussed in Ref. 14. In this work, we assume that when the radius of a circular capillary tube is smaller than a "threshold radius", r_p, the gas will condense in the tube and as a result, the condensate will form a liquid bridge provided $\sigma > \sigma_c$. Once a liquid bridge forms, it will grow. From the force balance:

$$h_1 = \frac{2\sigma}{\rho g r_1}(\cos\theta_R - \cos\theta_A) \quad \text{.......................... (5)}$$

where h_1 is the height of the liquid column when the gas pressure is constant and gas density is neglected. The advancing contact angle at the bottom interface θ_A can change from θ_{A0} to $\theta_{A\max}$, where $\theta_{A0} \geq \theta_R$ and $\theta_{A\max}$ is the limiting advancing contact angle; $\theta_{A0} \leq \theta_A \leq \theta_{A\max}$. We assume that the receding contact angle θ_R at the top interface is constant. When the length of the liquid column, h_1, exceeds $(2\sigma/\rho g r_1)(\cos\theta_R - \cos\theta_{A\max})$, it becomes unstable and moves downward to the end of the tube.

Liquid flow in the intersections. **Figs. 5a-h** depict the process of liquid formation, growth and flow in two connecting intersections. In this figure, the radii of the four intersecting ducts in intersection 1 and intersection 2 are r_1, r_2, r_3, r_4 and r_1', r_2', r_3', r_4' respectively. We assume that $r_2 < r_4$ and only $r_1 < r_p$; liquid first condenses in duct 1, and forms a liquid column, as shown in **Fig. 5a.**

Further gas condensation allows the length of the liquid column to increase, and the advancing contact angle will also increase. When the length of the liquid column, h_1, exceeds $(2\sigma/\rho g r_1)(\cos\theta_R - \cos\theta_{A\max})$, the liquid column becomes unstable and moves downward to the end of the duct at point A and stops. Due to the edge effect, the advancing angle θ_A continuously increases from $\theta_{A\max}$ to 90° at point A, as more liquid forms in duct 1. This causes the liquid height, h_1, to increase to a maximum, $(2\sigma/\rho g r_1)\cos\theta_R$ (see **Fig. 5b**). Further condensation causes the introduction of liquid to the intersection as shown in **Fig. 5c**, where the contact angle is θ_A. This step is accompanied by a small decrease in liquid height, h_1. With more liquid condensing, the liquid column in duct 1 increases its height back to the maximum, $(2\sigma/\rho g r_1)\cos\theta_R$ and finally the liquid in the intersection expands to a maximum radius $r_{\max}$. At $r_{\max}$, the liquid touches corner C (see **Fig. 5c**) and becomes unstable and 1) its interface may break into two new interfaces; one interface in duct 2, and the other interface in the intersection as shown in **Fig. 5d**; or 2) the liquid in duct 1 may flow down immediately to provide liquid for the new configuration shown in **Fig. 5e**. The expression for $r_{\max}$ is obtained by using a force balance:

$$r_{max} = \frac{2r_2 \cos\theta_{A\max} + \sqrt{4r_2^2 + r_3^2 \sin^2\theta_{A\max}}}{\sin\theta_{A\max}} \quad ..(6)$$

For the configuration in **Fig. 5d**, liquid flowing into duct 2 from duct 1 is determined from the new liquid column height in duct 1. From a force balance in duct 1 and duct 2, the maximum liquid height in duct 1 is found to be:

$$h_1' = \frac{2\sigma}{\rho g}\left(\frac{\cos\theta_R}{r_1} - \frac{\cos\theta_{A\max}}{r_2}\right) \quad ....(7)$$

provided $R = r_2 / \cos\theta_A$ (see **Fig. 5d**). Once the liquid pressure in the intersection exceeds the liquid pressure in duct 2, the configuration shown in **Fig. 5d** becomes unstable and the configuration in **Fig. 5e** develops

For the configuration shown in **Fig. 5e**, the fact that the liquid pressure in the interface may be higher than liquid pressure in duct 2, the liquid in intersection 1 is pulled into duct 2, until it breaks to two new interfaces in duct 1 and duct 2. When more gas condenses, the contact angle at the bottom interface of duct 1 changes from $\theta_{A\max}$ to 90° as the height of liquid column in duct 1 increases to $(2\sigma/\rho g r_1)\cos\theta_R$. If there is still more gas condensing in duct 1, the condensed liquid flows into duct 2 through the corner while the height of liquid column in duct 1 remains the same. As more gas condenses, the liquid fills duct 2, and the contact angles at both edges increase to 90°. Finally liquid enters intersection 2 as shown in **Fig. 5f**. The curvature of the liquid interface in intersection 1 changes to the convex shape and the maximum height of the liquid column in duct 1 increases to $(2\sigma / \rho g)(\cos\theta_R / r_1 + 1 / R_1)$ with further condensation. The liquid bridge in intersection 2 keeps growing until it touches corner D and breaks into new interfaces. The interface in intersection 1 also breaks to two new interfaces in ducts 1 and 2. If $r_1' < r_3'$, the stable configuration shown in **Fig. 5g(1)** realizes provided the liquid pressure in the intersection and duct 2 can be the same. If $r_1' > r_3'$, the new interface shown in **Fig. 5g(2)** with the dashed line is unstable. Liquid will be pulled into duct 3' and the stable configuration as shown with the solid line will evolve.

The interface in intersection 2 of **Fig. 5g(1)** with further condensation expands until it touches the other corner E, then it breaks to two new interfaces as shown in **Figs. 5h(1a)** and **5h(1b)**. The configurations in **Figs. 5h(1a)** and **5h(1b)** are for different duct sizes as shown in these figures. In **Fig. 5h(1a)**, with further condensation, duct 4' will be filled and then the vertical liquid column from ducts 1' and 3' will increase till it becomes unstable leading to the configuration in **Fig. 5i**.

When the liquid first forms in a horizontal capillary duct ($r < r_p$), the liquid bridge is stable until it reaches the intersections; then the contact angles at both edges increase to $90°$ (i.e., flat interface). There will be no further condensation on those flat interfaces. The maximum liquid length in a horizontal duct is the duct length.

In addition to the process described above, we also assume that when a liquid bridge first forms in a duct, it will appear in its middle. When two liquid bridges have been established in a single duct as result of flow from the neighboring ducts, these two liquid bridges upon touching each other form a single bridge or column. The rules governing the stability of a liquid column or a liquid bridge are based on the force balance which is the same as relating the pressures at various points in a liquid medium; in the horizontal direction, liquid pressure should be the same in a continuous liquid medium, and in the vertical direction, liquid pressure should be in hydrostatic equilibrium.

Network specification. We represent the porous media by a two-dimensional vertical square network with randomly sized circular capillary ducts. In this work, we use a network with dimensions of 20 x 20 intersections. The radius of each duct is randomly chosen from a log-normal size distribution function, shown in **Fig. 6**. The average radius of the ducts is 23.06 μm, and the standard deviation is 5.74. For simplicity, we assume each capillary duct has the same length, $l = 6000\ \mu m$. The total PV of the network is 8.89 mm^3. **Fig. 7** provides the network used in this work. The thickness of the lines is proportional to the duct diameter.

Procedure and results. Initially, the network is fully saturated with gas at a pressure above the dew point pressure. The gas pressure is then decreased to allow the liquid to form. In our simulation, we modify the continuous condensation process with discrete steps. During every step, a small amount of liquid forms. At the saturation point, those ducts with $r < r_p$ allow condensation in the form of a liquid bridge. Later on those ducts with radii larger than r_p which contain liquid bridges also serve as condensation sites. In this work, r_p is assumed to be 20 μm, and the amount of condensation per step in a liquid bridge is $200\ \mu m^3$. For simplicity we keep surface tension constant and assume that it is independent of pressure. This restriction on surface tension can be easily removed. We also assume that the gas pressure is constant in the entire network and the effect of gas pressure on the gas-liquid interface is also neglected.

Fig. 8 shows the liquid distributions in the network for $\theta_R = 0°, \theta_{A\max} = 10°, \rho = 0.5\ g/cm^3, \sigma = 0.1\ dyne/cm$ at various stages of pressure depletion where liquid condensation increases.

Fig. 8a shows the condensate distribution in the network at $T = 10{,}000$ steps. The condensate saturation is 5.62%. Only small ducts have formed liquid bridges. There is little difference in condensate volume between vertical and horizontal ducts. This means that the liquid in most vertical ducts is still stable.

Fig. 8b shows the condensate distribution in the network at $T = 25{,}000$ steps. At this stage, the condensate saturation is $S_c = 16.6\%$. The small ducts and some nearby large ducts have formed liquid bridges, but the condensate is not well connected to the outlet.

Fig. 8c shows the condensate distribution in the network at $T = 35{,}183$ steps. At this stage, the condensate paths have been well established, the liquid is mobile, and the network produces condensate at a stable rate. The saturation is $S_c = 26.0\%$. Critical condensate saturation is defined as the liquid saturation at which the liquid production from the network becomes sustainable. Thus, in **Fig. 7c** the network has reached critical condensate saturation.

Critical condensate saturation, S_{cc}, of the network is obtained from

$$S_{cc} = \frac{V_{total} - V_{out}}{PV} \quad \text{..} \quad (8)$$

where V_{total} is the total liquid condensed in the network, V_{out} is the total liquid production of the network, and PV is the total porous volume. For this example, $V_{total} = 2.31\ mm^3$, $V_{out} = 7.25 \times 10^{-5}\ mm^3$ and $PV = 8.89\ \ mm^3$.

Effect of various parameters. Fig. 9 displays the calculated results for critical condensate saturation, S_{cc}, for various values of surface tension and contact angle hysteresis. The calculations are based on the 20×20 intersections network described above. The figure reveals that surface tension has a pronounced influence on critical condensate saturation. As surface tension increases, critical condensate saturation also increases. The effect of contact angle hysteresis is somewhat different. Contact angle hysteresis, when $\theta_R = 0°$, and $\theta_{A\max}$ varies from $1°$ to $10°$ affects critical condensate saturation (**Fig. 9a**). However, contact angle hysteresis within the range of $10°$ to $30°$ seems to have a small effect on S_{cc}. The oscillations in S_{cc} for low values of surface tension are believed to be due to the network size (see **Fig. 9b**).

In order to study the sensitivity of the model to the network size, we increased the network size to 40×40 intersections. The advancing (maximum) and receding contact angles are $\theta_{A\max} = 20°$ and $\theta_R = 0°$. Other parameters are kept the same. The results of S_{cc} calculations are provided in **Fig. 10**. There is little effect of network size on S_{cc} values at high values of surface tension. The oscillations at low values of surface tension are due to the network size.

S_{or} in a network

Many authors discuss the displacement process by using a wide variety of network models. Here, the simple network described above is also used to study two-phase displacement to establish S_{or}. The network for displacement is similar to the one used by Lenormand et al [15]; we use circular tubes rather than the rectangular tubes.

Similar to Lenormand et al's model, the imbibition displacement follows the rules that: 1) in any duct, if the capillary pressure is equal to or higher than the invasion pressure, the invading liquid enters the duct and stops at the other end; 2) every duct is either full of wetting phase or non-wetting phase. (i.e. piston-type motion as shown in **Fig. 11a**); 3) snap-off motion occurs only when the piston-type motion is not possible for topological reasons as shown in **Figs. 11b, 11c**; 4) when the non-wetting fluid is in one duct at the intersection, the imbibition I1-type motion occurs as shown in **Fig. 11d**; 5) when the non-wetting fluid is only in two adjacent ducts at the intersection, the imbibition I2-type motion occurs as shown in **Fig. 11e**.

Procedure and results. In our S_{or} network model, we first perform a major drainage, then decrease the capillary pressure by increasing the water pressure to accomplish imbibition. From the drainage-imbibition process, we can determine residual oil saturation. The effect of gravity on S_{or} is neglected.

We separate the ducts in the network into seven groups according to their sizes, as shown in **Table 1**. Initially, the network is fully saturated with water (i.e., wetting phase).

The water reservoir is connected to the network at the top boundary. The oil (non-wetting phase) reservoir is connected to the network at the bottom boundary.

In the drainage process, oil is the invading phase while water is the invaded phase. We increase the oil reservoir pressure, P_o, and keep the water reservoir pressure, P_w, constant. At first, the oil pressure is increased gradually to the extent that it can enter the ducts which have sizes among groups 4 to 7. The oil phase does not form continuous paths to the top outlet at this pressure. We then increase the oil pressure to drain water in the ducts which have sizes in group 3. The oil at this pressure builds continuous paths to the top outlet. The oil pressure again is increased to allow water to be drained from all the ducts in which their paths have not been blocked. Some water is trapped no matter how much we increase the oil pressure. The trapped water is the residual water, and the water saturation is residual water saturation, S_{wr}. This is the end of the major drainage process.

After this initial drainage, we start an imbibition process where water is the invading phase and oil is the invaded phase. We keep increasing the water reservoir pressure, P_w, while keeping the oil reservoir pressure, P_o, constant. As we increase water pressure gradually, the capillary pressure allows water to enter the network. First, only piston-type displacement happens. We then increase water pressure further which causes the snap-off, imbibition I1- and I2-types displacements. When all the oil left in the network is the trapped oil, the imbibition process ends, and the oil saturation is residual oil saturation, S_{or}.

In order to investigate the relationship between S_{or} and surface tension, we change the surface tension and repeat the drainage-imbibition process; S_{or} values at different surface tensions are obtained which are shown in **Fig. 12**. The figure reveals that when surface tension is lower than 0.25 *dyne/cm*, S_{or} increases with increasing surface tension. When surface tension is higher than 0.25 *dyne/cm*, S_{or} is independent of surface tension. **Fig. 13** shows residual oil saturation for a low water-oil interfacial tension of 0.25 *dyne/cm* ($S_{or} = 48.5\%$). Note the end effects on the right and left sides cause the oil to be trapped. Comparison of this figure with **Fig. 8** reveals that S_{or} and S_{cc} are different entities.

Discussion and conclusions

In this work, we have used simple tube geometries and a simple network for the representation of porous media. With these simple geometries, surface tension and contact angle hysteresis are key parameters of the critical condensate saturation model. Surface tension for gas condensate systems is often known. However, the current knowledge on contact angle hysteresis for gas condensate systems on a rock substrate is very little. Since a rock substrate is not smooth, one may expect contact angle hysteresis. In reservoir engineering calculation, it is often assumed that the contact angle between the oil and gas phases on a rock substrate is zero (θ measured through the oil phase). However, this does not mean that the contact angle hysteresis is zero. Very simple laboratory experiments using capillary tubes in the vertical position reveal that liquid in equilibrium with its vapor does not flow. The only reason for the liquid holdup is the contact angle hysteresis. Since contact angle hysteresis may depend on the type of hydrocarbons, one may speculate that the contact angle hysteresis for a model fluid such as C_1/nC_4 and an actual condensate may not be the same.

The phenomenological model described in this paper leads to the following conclusions:

1. Critical condensate saturation, S_{cc}, in a network of circular capillary tubes is similar to that of a single tube; S_{cc} increases with an increase in surface tension.

2. Critical condensate saturation in a network of capillary tubes is affected by contact angle hysteresis within the range of $0°$ to $10°$; when contact angle hysteresis increases, S_{cc} also increases. S_{cc} is only slightly affected by the contact angle hysteresis in the range of $10°$ to $30°$.

3. There is an essential distinction between critical condensate saturation, S_{cc}, and residual nonwetting saturation, S_{or}. Above a certain value of surface tension, S_{or} is independent of this parameter in a capillary tube network. However, S_{cc} is a function of surface tension both in a capillary tube network and in a single tube.

The above conclusions are based on the balance between the capillary and gravity forces for S_{cc}. The conclusions, will, therefore, apply to critical condensate saturation in a vertical system, where viscous forces are neglected. S_{cc} in the horizontal direction when viscous forces are applied requires the examination of pressure effects, which are not covered in this work.

Nomenclature

a = *side length of an equilateral triangular tube*

A = *liquid cross-section area*

l = *duct length*

l_1 = *parameter defined by Eqs. A-4 and A-15*

l_2 = *parameter defined by Eqs. A-5 and A-16*

h = *height of liquid bridge*

P = *pressure*

P_c = *capillary pressure*

PV = *pore volume*

r = *radius of a tube, also radius of the side curve of curved triangle*

R = *radius of interface*

r_p = *threshold radius*

S = *saturation*

S_{cc} = *critical condensate saturation*

S_{or} = *residual oil saturation*

S_{cr} = *critical gas saturation*

V = *volume of condensate*

Greek letters

α = *angle defined for a curved triangular tube*

θ = *contact angle*

θ_c = *critical contact angle*

ρ = *density*

$\Delta\rho$ = *density difference between liquid and gas phases*

σ = *surface tension*

σ_c = *critical surface tension (corresponding to* $\theta_c = 0°$)

Subscripts

A = *advancing*

C = *condensate*

CC = *critical condensate*

max = *maximum*

out = *liquid flowing out of the network*

R = *receding*

$total$ = *total condensate that has been condensed*

References

1. Cahn, J. W.: "Critical Point Wetting," *Journal of Chemical Physics* (1977) **66**, 3667-72
2. Williams, J. K., and Dawe, R. A.: "Near-Critical condensate Fluid Behavior in Porous Media - A Modeling Approach," *SPE Reservoir Engineering* (May 1989) 221-227.
3. Firoozabadi., A., and Kashchiev, D.: "Pressure and Volume Evolution During Gas Phase Formation in Solution Gas Drive Process," *SPE Journal* (Sept. 1996)
4. Saeidi, A., and Handy, L. L.: "Flow and Phase Behavior of Gas Condensate Volatile Oils in Porous Media," SPE 4891, Society of Petroleum Engineers, 1974.

5. Gravier, J. F., Lemouzy, P., Barroux, C., and Abed, A. F.: "Determination of Gas-Condensate Relative Permeability on Whole Cores Under Reservoir Conditions," *SPE Formation Evaluation J.* (Feb. 1986) 9-15.

6. Danesh, A., Henderson, G. D., and Peden, J. M.: "Experimental Investigation of Critical Condensate Saturation and its Dependence on Interstitial Water Saturation in Water-Wet Rocks," *SPE Reservoir Engineering* (Aug. 1991) 336-342.

7. Chen, H. L., Wilson, S. D., and Monger-McClure, T. G.: "Determination of Relative Permeability and Recovery for North Sea Gas Condensate Reservoirs," SPE 30769, Society of Petroleum Engineers, 1995.

8. Munkerud, P. K., and Toaster, O.: "The Effects of Interfacial Tension and Spreading on Relative Permeability in Gas Condensate Systems," Eighth European Symposium on Improved Oil Recovery, May 15-17, 1995, Vienna, Austria.

9. Princen, H. M.: "Capillary phenomena in Assemblies of Parallel Cylinders," (part 1), *Journal of Colloid & Interface Sci.* (1969) 69-75.

10. Princen, H. M.: "Capillary phenomena in Assemblies of Parallel Cylinders," (part 2), *Journal of Colloid & Interface Sci.* (1969) 359-368.

11. Princen, H. M.: "Capillary Pressure Behavior in Pores with Curved Triangular Cross Section: Effect of Wettability and Pore Size Distribution," *Journal of Colloid & Interface Sci.* (1992) 221-230.

12. Mason, G., and Morrow, N. R.: "Capillary Behavior of a Perfectly Wetting Liquid in Irregular Triangular Tubes," *Journal of Colloid & Interface Sci.* (1991) 262-273.

13. Defay, R., and Prigogine, I.: *Surface Tension and Adsorption*, Longmans, London (1966) **Chapter XV and XVI.**

14. Firoozabadi, A.: *Advanced Thermodynamics of Hydrocarbon Reservoirs*, **Chapter 2,** (in preparation).

15. Lenormand, R., Zarcone, C., and Sarr, A.: "Mechanisms of the Displacement of One Fluid by Another in a Network of Capillary Duets," *Journal of Fluid Mech.* (1983) 337-353.

Appendix: Critical Condensate Saturation (Liquid Holdup) Expressions

In the following derivations, the tube is assumed in a vertical position. First we will derive the expression for liquid holdup in an equilateral-triangular tube.

Triangular tube. Let's first derive the expressions for capillary rise in an equilateral triangular tube shown in **Fig. 3** of the text (see **Figs. 3a** and **3b**). For simplicity we will limit the derivations for $\theta < 60°$. **Fig. 3a** depicts the vertical cross section across AD. The horizontal cross-section is shown in **Fig. 3b**. We assume that the interface is near-vertical for $h > h_1$, similar to the assumption made by Princen. [9] When the whole column is at equilibrium, the force balance on the liquid column below $h = h_1$ is given by:

$F_s = F_G$ .... (A-1)

where the interfacial force F_s is given by

$F_s = \sigma(l_1 \cos\theta + l_2)$ .... (A-2) and the gravity force F_G is given by

$$F_G = \Delta\rho g h_1 A_{h1} \text{ .... (A-3)}$$

In Eq. A-3 the gas density is neglected. l_1 is the length of the nonwetting phase-wetting phase interface in contact with the solid wall, and l_2 is the length of the wetting phase in contact with the nonwetting phase and A_{h1} is the liquid cross-section area of the interface at $h = h_1$. From **Fig. 3b**

$$l_1 = 3\left[a - 4R_1 \sin\left(\frac{\pi}{3} - \theta\right)\right] \text{ .... (A-4)}$$

$$l_2 = 3\left(\frac{2}{3}\pi - 2\theta\right)R_1 \text{ .... (A-5)}$$

$$A_{h1} = \frac{\sqrt{3}}{4}a^2 - 3R_1^2\left[\sqrt{3}\cos^2\theta - \sin\theta\cos\theta - \left(\frac{\pi}{3} - \theta\right)\right]$$

$$\text{.. (A-6)}$$

The radius R_1 in **Fig. 3b** is given by the capillary pressure at $h = h_1$

$$P_{c1} = \Delta\rho g h_1 = \frac{2\sigma}{R_1} \text{ .... (A-7)}$$

Combining Eqs. A-1 to A-6 provides the expression for R_1

$$R_1 = \frac{a}{2\sqrt{3}\cos\theta} \text{ .... (A-8)}$$

The expression for h_1 is then readily obtained through $h_1 = 2\sigma/\Delta\rho g R_1$.

The next step is to obtain an expression for h, the liquid column in the vertical triangular tube (see **Fig. 4**). The basic concepts are the same as the capillary rise. There is a need to incorporate contact angle hysteresis so that the tube can hold a liquid column. We have to write the basic expression

$$P_{cA} = P_{cR} + \Delta\rho g h \quad \text{(A-9)}$$

where P_{cA} is the capillary pressure on the advancing meniscus and P_{cR} is the capillary pressure at the receding meniscus. Substitution of various parameters with appropriate contact angles in Eq. A-9 will provide Eq. 3 of the text.

Curved triangular tube. The capillary rise in an equilateral curved triangular tube is similar to that for an equilateral triangular tube but somewhat more complicated. **Fig. 3a** and **Fig. 3c** show the two cross sections. In the following, the derivations will be for a positive P_c.

The capillary pressure at $h = h_1$ (see **Fig. 3a** and **Fig. 3c**) is given by:

$$P_{c1} = 2\sigma/R_1 = \Delta\rho g h_1 \quad \text{(A-10)}$$

R_1 is obtained

$$R_1 = \frac{1-\cos\alpha_1}{\cos(\alpha_1+\theta)} r \quad \text{(A-11)}$$

where r is the radius of the curved triangle, and α_1 is obtained from

$$(\frac{\sqrt{3}}{3} - \frac{\pi}{6}) - (2-\cos\alpha_1)\sin\alpha_1 - (1-\cos\alpha_1)^2 \tan(\alpha_1+\theta)$$

$$+\alpha_1 - \left(\frac{\pi}{6} - \alpha_1\right)\cos\theta \frac{(1-\cos\alpha_1)}{\cos(\alpha_1+\theta)} = 0 \text{ .... (A-12)}$$

To obtain the capillary holdup height h in a curved-triangular tube, the force balance equations at the interfaces on both sides are written

$$F_{P_{cn}} = F_{sn} \text{ .... (A-13)}$$

$$F_{P_{cn}} = P_{cn}A_n \text{ .... (A-14)}$$

where $n = A, R$; A and R represent advancing and receding interfaces, respectively and $F_{P_{cn}}$ is the capillary force balanced by the interfacial force F_{sn}. The expression for F_s is given by Eq. A-2 and parameters l_{1n}, l_{2n}, A_n ($n = A, R$) are given by

$$l_{1n} = 3r(\frac{\pi}{3} - 2\alpha_n) \text{ .... (A-15)}$$

$$l_{2n} = 3r[\pi - 2(\alpha_n + \theta)]\frac{1-\cos\alpha_n}{\cos(\alpha_n+\theta)} \text{ .... (A-16)}$$

$$A_n = (\sqrt{3} - \frac{\pi}{2})r^2 - 3r^2[(2-\cos\alpha_n)\sin\alpha_n + (1-\cos\alpha_n)^2$$

$$\tan(\alpha_n+\theta) - (\frac{\pi}{2} - (\alpha_n+\theta))\frac{(1-\cos\alpha_n)^2}{\cos^2(\alpha_n+\theta)} - \alpha_n] \text{ (A-17)}$$

Once the receding and advancing parameters are known, Eq. A-9 is used to obtain Eq. 4 of the text.

TABLE 1 -- Different Groups of Radii (μm)

Group 1	less than 10
Group 2	10 to 15
Group 3	15 to 20
Group 4	20 to 25
Group 5	25 to 30
Group 6	30 to 35
Group 7	larger than 35

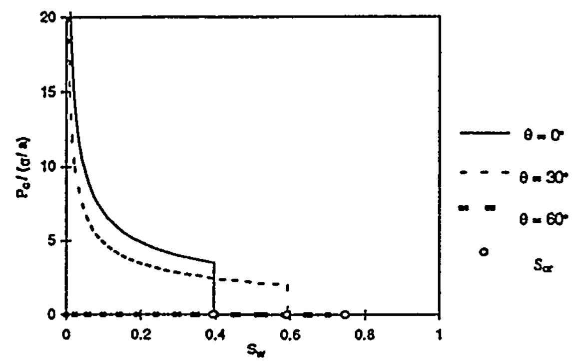

(a) -- Equilateral triangle

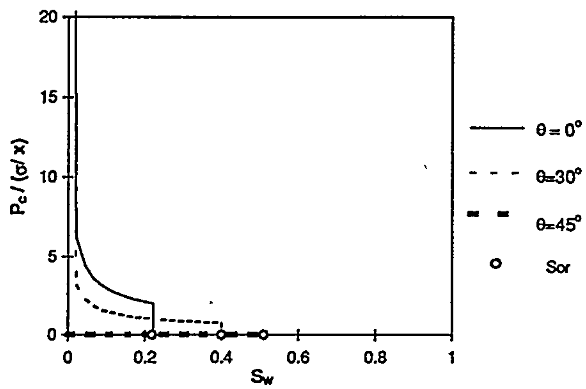

(b) -- Square

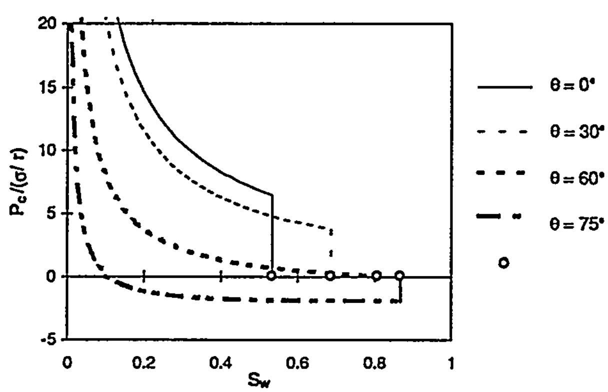

(c) -- Curved triangle

Fig. 1 -- Imbibition P_c-S_w plots for a single tube of different shapes

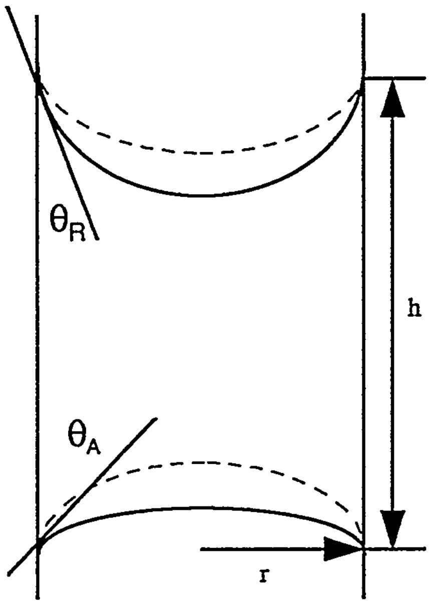

Fig. 2 -- Advancing and receding interfaces of a liquid column in a Circular capillary tube

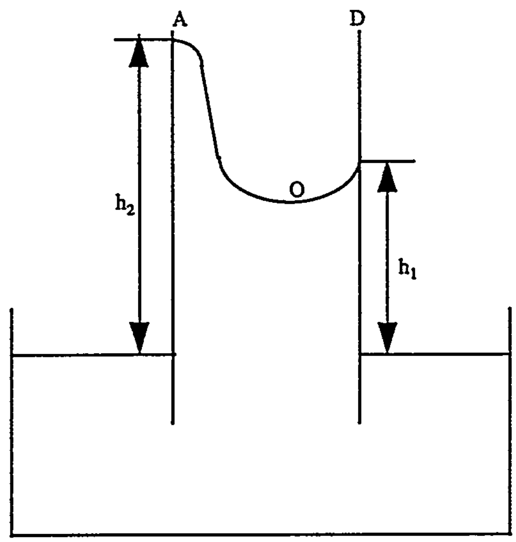

(a) Capillary rise in a triangular and curved triangular tube

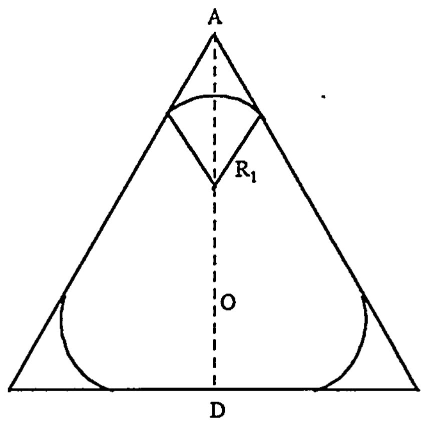

(b) Cross-section of liquid-gas interface in an equilateral triangular tube at $h=h_1$

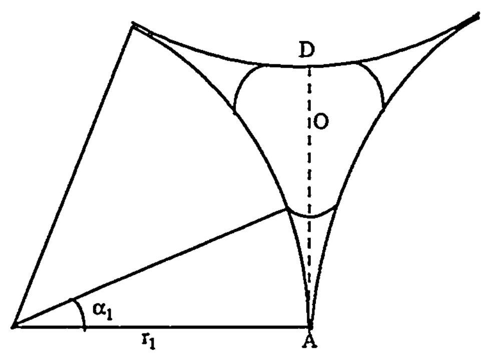

(c) Cross-section of liquid-gas interface in an curved triangular tube at $h=h_1$

Fig. 3 -- Capillary rise in triangular and curved triangular tubes

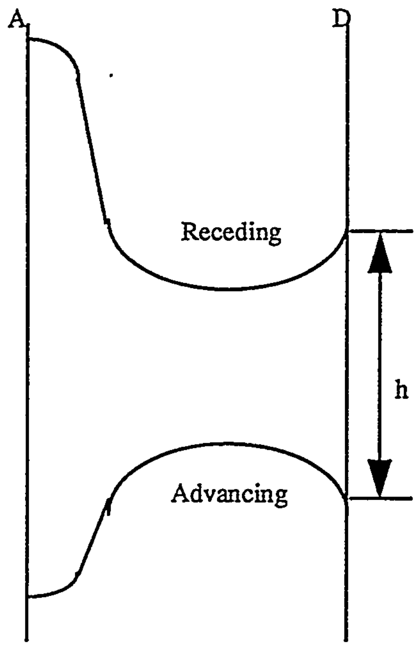

Fig. 4 – Liquid holdup in a triangular or curved triangular tube

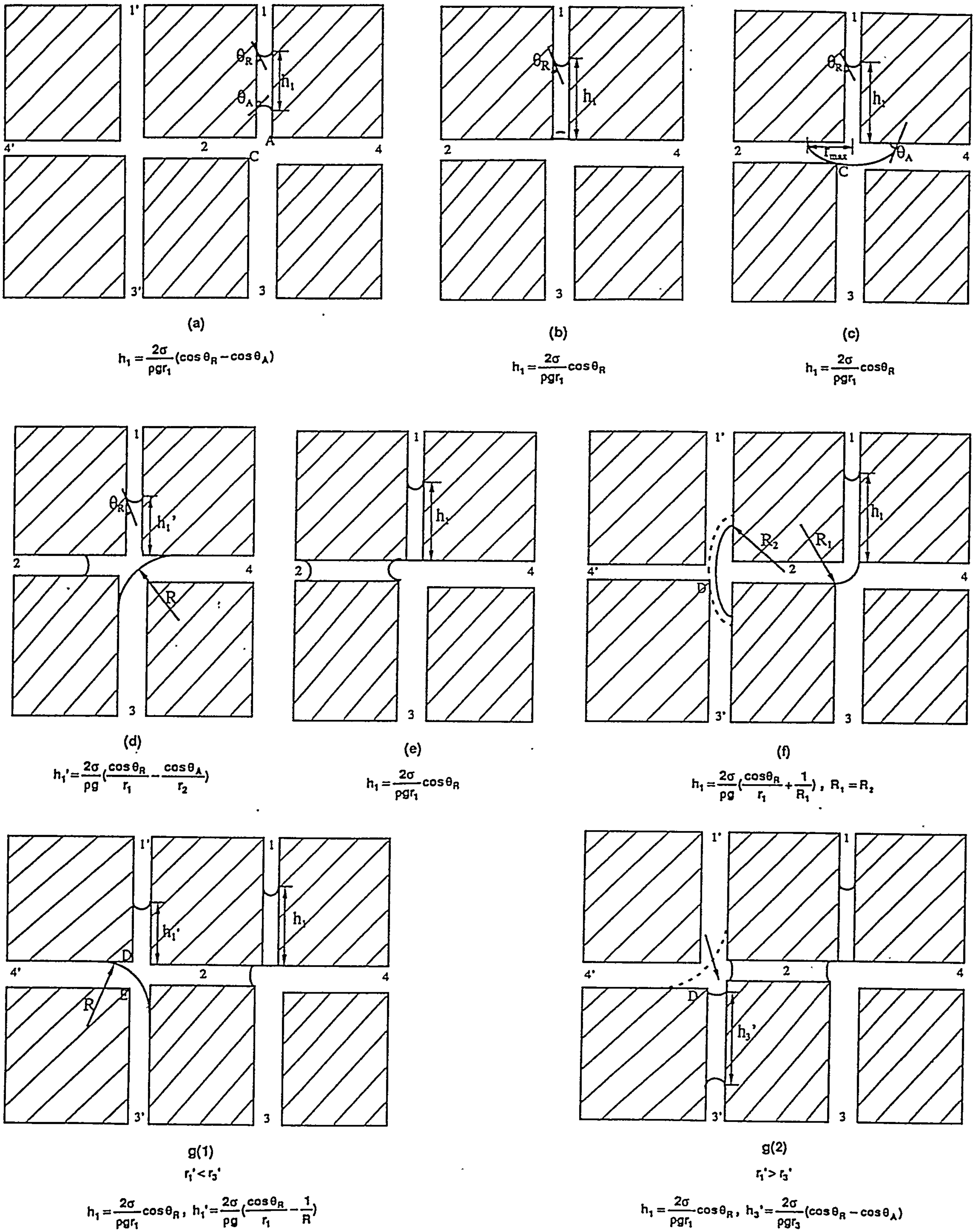

Fig. 5 – Schematics of liquid formation and flow in intersections

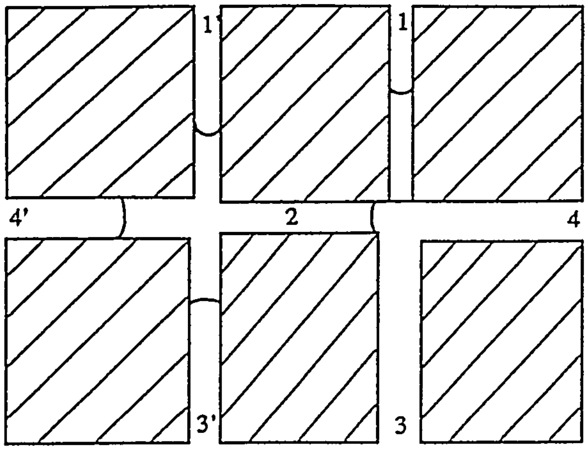

h(1a)

$r_3' > r_1'$, $r_4' > r_2$

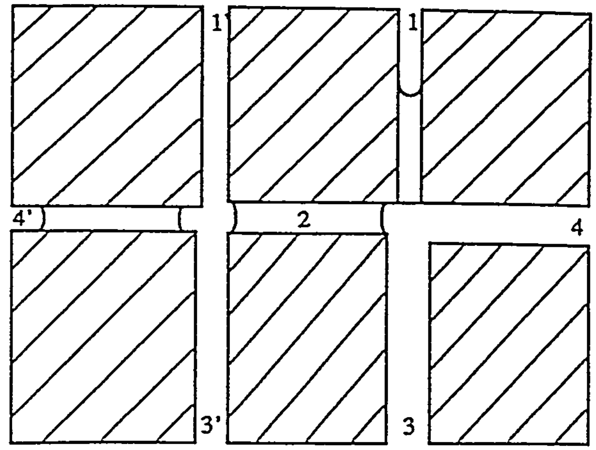

h(1b)

$r_3' > r_1'$, $r_4' < r_2$

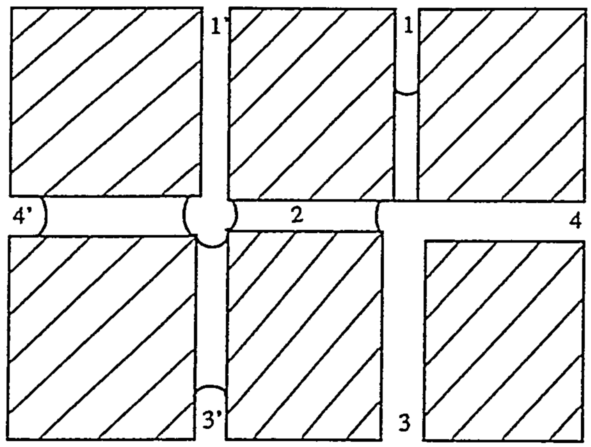

i

$r_3' > r_1'$, $r_4' > r_2$

Fig. 5 – (Continued)

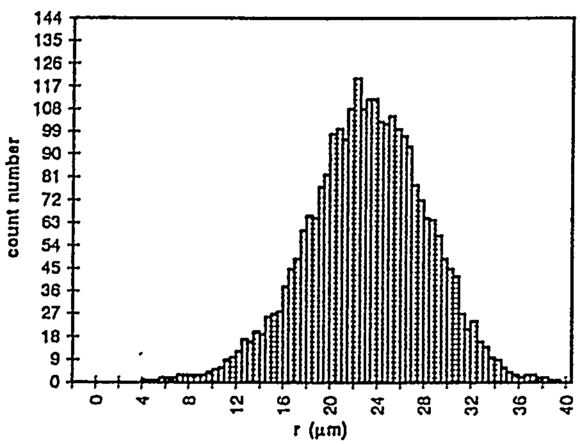

Fig. 6 – Radii's distribution of the network

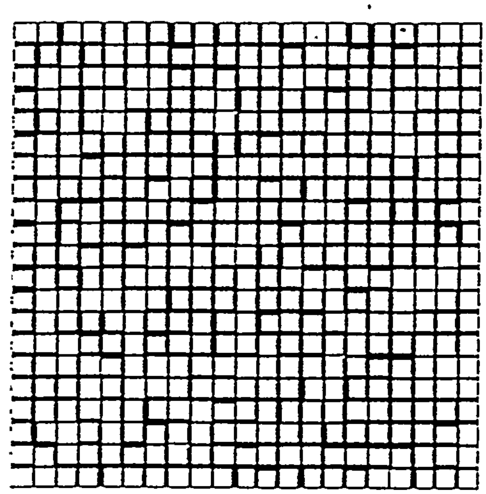

Fig. 7 – Network size distribution of 20x20

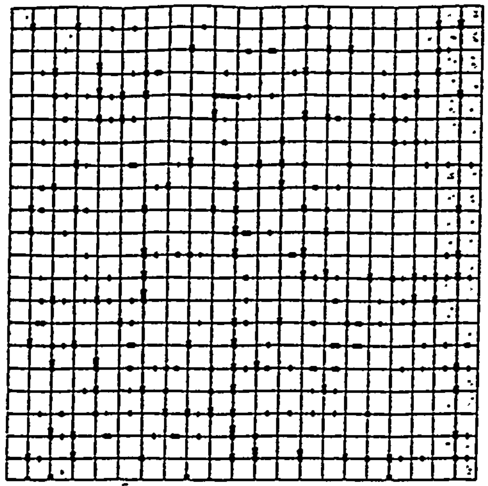

(a) T = 10,000, S_e = 5.62 %

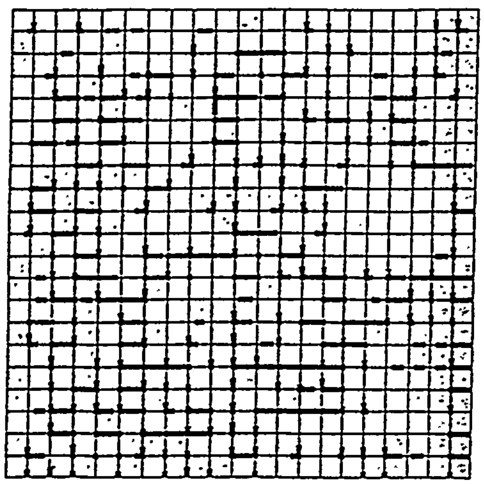

(b) T = 25,000, S_e =16.6 %

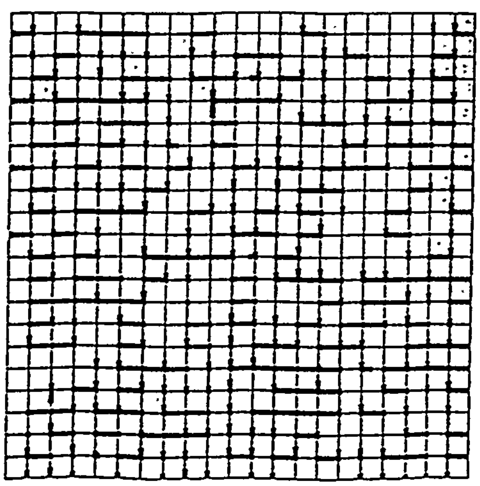

(c) T = 35,183, S_c = 26.0 %

Fig. 8 – Liquid distributions at different stages of condensation
$\sigma = 0.1$ dyne / cm , $\rho = 0.3$ g / cm^3 , $\theta_R = 0°$, $\theta_A = 10°$

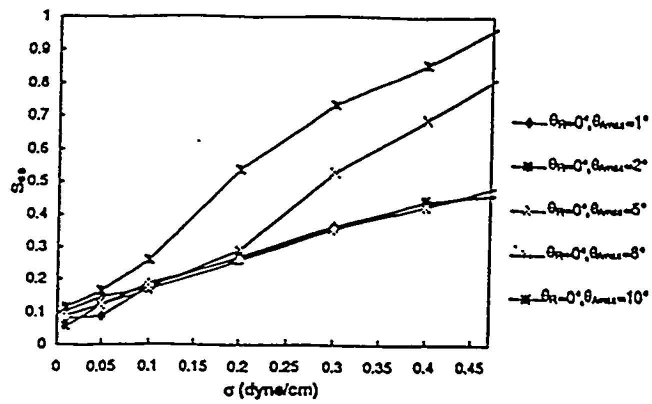

(a) – Contact angle hysteresis ≤ 10°

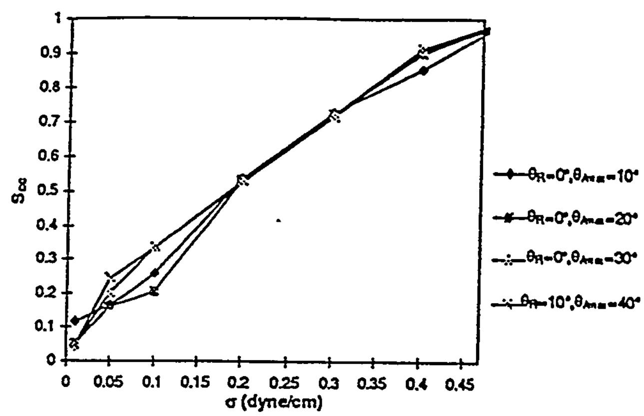

(b) – Contact angle hysteresis ≥ 10°

Fig. 9 – S_{cc} vs. surface tension at different contact angle hysteresis network sizes 20 x 20

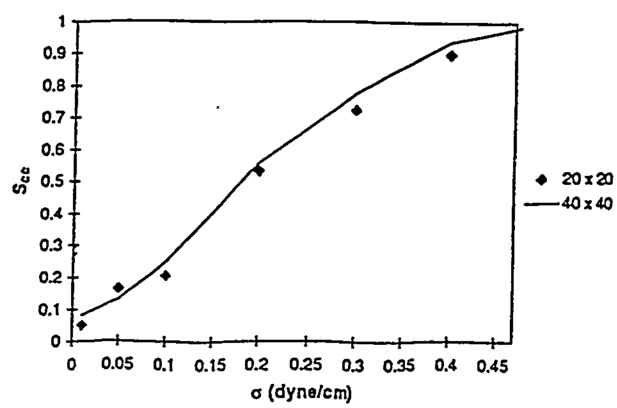

Fig. 10 – S_{cc} vs. surface tension for two different network sizes

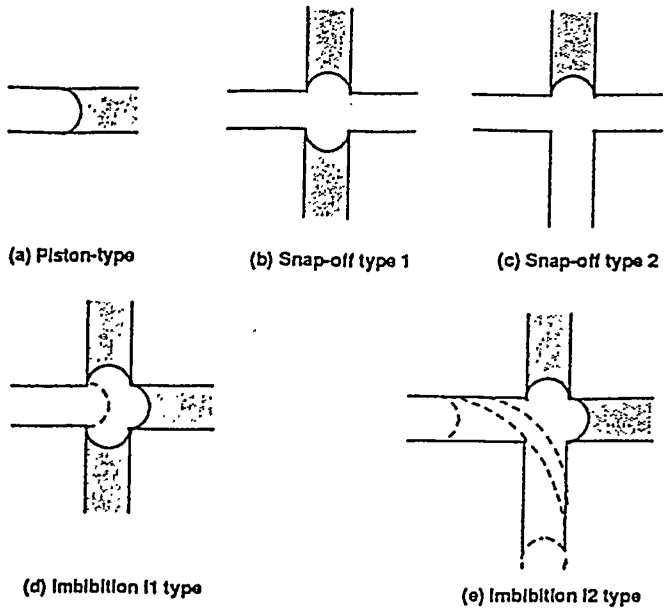

Fig. 11 – Basic mechanism of imbibition (after Lenormand, et al)

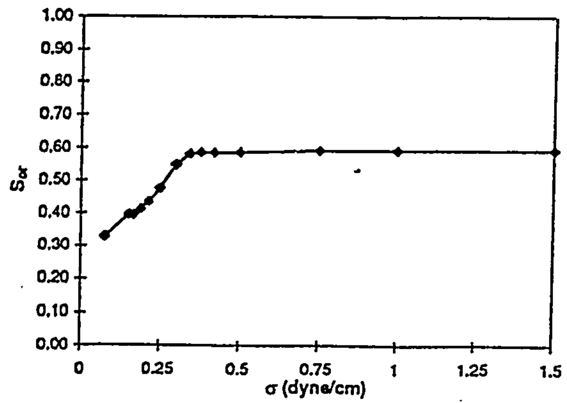

Fig. 12 – S_{or} vs. surface tension

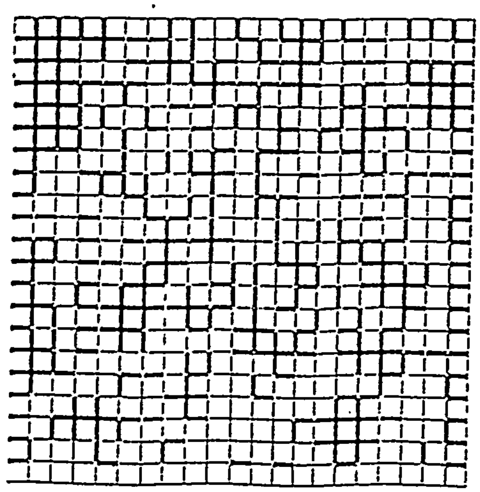

Fig. 13 – Liquid distribution at the end of imbibition